A Radiation-Hardened Neuromorphic Imager with Self-Healing Spiking Pixels and Unified Spiking Neural Network for Space Robotics

Quan Cheng[1,2], Qiufeng Li[1], Zhengke Yang[1], Zhen Kong[1], Gaoqiang Niu[1], Yuan Liang[1], Jiamin Li[1], Jeong Hoan Park[3], Wang Liao[4], Hiromitsu Awano[2], Takashi Sato[2], Longyang Lin[*1], Masanori Hashimoto[*2]

[1]Southern University of Science and Technology, Shenzhen, China, [2]Kyoto University, Kyoto, Japan, [3]Kyung Hee University, Gyeonggi, South Korea, [4]Kochi University of Technology, Kochi, Japan (*Corresponding authors)

Abstract

A radiation-hardened neuromorphic imager prototype is developed for space exploration, featuring a fully spike-based neuromorphic vision system architecture, in-pixel self-healing against radiation-induced damage, and integrated unified spiking neural network (USNN) with adaptive neurons and synapses and contrast enhancement at low-contrast conditions. Self-healing reduces dark current by 6.25× at 14kGy cumulative dose, recovering recognition accuracy by 27.8%. USNN consumes 0.0529 pJ/SOP at 5,000 events/s.

Introduction

Space-grade ICs are in constant demand in view of the continuous interest in space exploration [1]-[8], where the operating environment challenges silicon systems (e.g., radiation from cosmic rays induces damage and faults, extreme lighting conditions limit the harvested power from solar panels). Such harsh conditions mandate high radiation tolerance, low power consumption, and resilient processing in space ICs (Fig.1). For space image sensors, radiation causes total ionizing dose (TID) and displacement damage dose (DDD) in CMOS pixels [9]-[10], resulting in faulty responses and hot pixels with high dark current [11]-[14]. Voltage compensation has been used to mitigate these effects but requires high voltages (9-30V) and significant power (>0.2W) [11]. While silicon carbide (4H-SiC) photodiodes (PDs) offer strong radiation tolerance, their quantum efficiency in the visible range is limited [14]. Techniques like gate-overlap PDs and enclosed layout transistors [11]-[13] can enhance radiation tolerance but fail to recover damaged pixels, thus not extending the actual pixel lifetime. Annealing can effectively repair radiation-induced lattice damage, but heating the full sensor incurs significant power [15]. Furthermore, conventional pixel readouts [11]-[14], relying on analog sampling and conversion, are susceptible to transient faults from radiation-induced charge fluctuations and signal distortions, while also lacking the processing capability required for image enhancement and advanced space exploration tasks. Imagers incorporating CNNs [16] or BNNs [17] add intelligence but remain susceptible to radiation in space.

Proposed Neuromorphic Imager

This work presents a radiation-hardened neuromorphic imager for space robotics (Fig.2), featuring: 1) a fully spike-based vision system, which eliminates the need for ADCs, enhances resilience to radiation-induced faults, and achieves state-of-the-art energy efficiency; 2) radiation-hardened pixel array with in-pixel localized annealing, enabling self-healing against radiation damage; 3) integrated unified spiking neural network (USNN) incorporating adaptive excitatory and inhibitory (E/I) neurons and synapses for space object recognition and spatialization; and 4) spike-based time-domain exponential (STE) contrast enhancement for low-light conditions. Key feature demonstrations are shown in Fig.3.

The system (Fig.2) consists of a 73×73-pixel array, a USNN, pixel readout, controller, and an SPI interface. The pixel array generates spike signals with frequencies representing light intensity, which are directly fed into the USNN with three task-specific output heads for terrain recognition, object positioning, and focus state analysis. Each USNN layer processes spikes using digital counters, multiplying binary weights (-1, +1) and firing output spikes to the next layer. The distributed nature of spikes offers inherent redundancy and resilience [18]-[22], making our system more fault-tolerant than traditional sampling-based systems.

Triple module redundancy (TMR) registers are used for weight storage, but TMR proves less effective for CMOS pixels, which are susceptible to cumulative long-term radiation damage. Accelerated alpha irradiation tests reveal significant hot pixels at doses exceeding 10kGy, with dark current increases of ~10,000× (Fig.1, bottom). To address this, in-pixel annealing is introduced to enable localized thermal recovery of silicon's electrical properties. Fig.4 shows the pixel design integrating spike generation and self-annealing. The PD is an N+/P- well diode with an extra N-well guard ring for enhanced radiation tolerance. Spike generation is achieved through a positive feedback loop, where photocurrent from reversed-biased PD alternately charges and discharges the Schmitt-trigger buffer, producing output pulses with frequencies proportional to light intensity [18]. In self-annealing, the PD is forward biased by the column driver, creating a local hot spot (>120°C @ 2V) for annealing with minimized power overhead.

USNN (Fig.5, top) begins with STE modules for synaptic integration. A synchronizer aligns asynchronous pixel spikes before aggregation, firing spikes to subsequent layers when thresholds are exceeded. To enhance energy efficiency, adaptive E/I neurons and synapses inhibit irrelevant neurons and synapses using clock gating (Fig.5, bottom). For low-light conditions commonly encountered in space exploration, STE contrast enhancement exponentially accumulates pixel spikes during synaptic integration via shifters (Fig.6, top and Fig.3(c)).

Measurement Results

The proposed 180nm design (Fig.10) exhibits excellent spike frequency linearity with light intensity, achieving an R^2 value of 99.7% (Fig.7, top). Under low-light conditions (~100 lux), STE contrast enhancement improves inference accuracy by 57.8%-63.1% and inference speed by 3.3×. The USNN operates at 200 kHz to match the highest spike frequency and consumes 59 μW at 0.6V during recognition and spatialization tasks for the Mars surface images dataset (Fig.6, bottom). Adaptive E/I neurons and synapses reduce USNN power consumption by 31.2% with 61.83% of synapses inhibited, achieving a system energy (including pixel array) of 0.0529 pJ/SOP (18.9 TSOPS/W), marking a 51-to-639× improvement over previous SOTA imagers (Table.I). Accelerated alpha irradiation experiment is performed using Americium-241 with a radioactivity of 4 Mbq (significantly exceeding typical space conditions, Fig.8). During in-pixel localized annealing, the local power density ranges from 0.11 to 0.47 mW/μm² at 1.5-2.5V, reaching temperatures above 120°C at a typical voltage of 2.0V (Fig.8, bottom). Damaged pixel recovery was evaluated under varying radiation doses, demonstrating both quick recovery within 3 minutes and repeated recovery (Fig.9, left). In repeated recovery, after four rounds of accelerated irradiation and annealing, self-healing pixels show a dark current increase rate that is 6.25× slower than untreated pixels, effectively extending the device lifespan. As cumulative doses increase, the number of damaged pixels rises, degrading USNN accuracy. By applying self-healing, the USNN accuracy is recovered by 27.8% under 14kGy irradiation (Fig.9, right).

Acknowledgements This work was supported in part by the Nat'l Natural Science Foundation of China under Grant 62274081; the Grant-in-Aid for Scientific Research (S) from JSPS under Grant 24H00073; Zhujiang Young Talent Program (Grant 2023QN10X177).

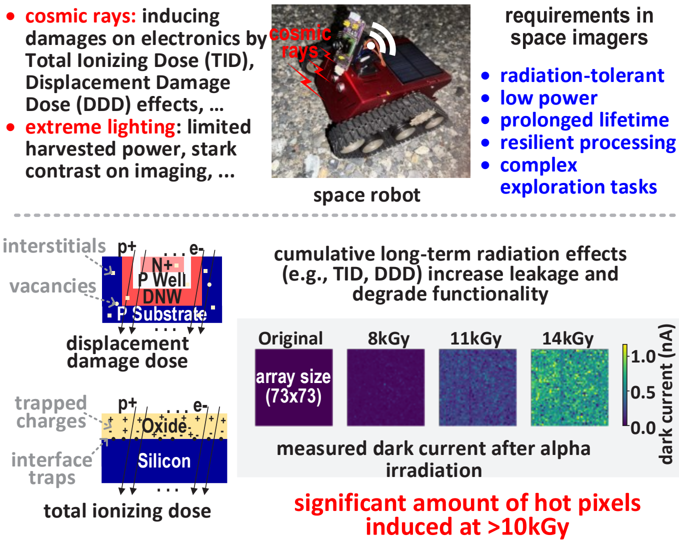

Fig. 1. Overview of challenges and requirements for imagers in space robotics (top) and the cumulative long-term radiation effects on imagers (bottom).

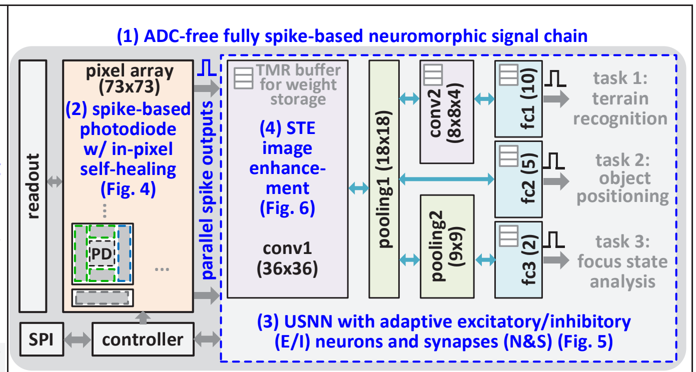

parameter		features enabling high radiation tolerance, low power, and intelligent space imaging
radiation-hardening	soft-errors	- fully spike-based neuromorphic system (ADC-free) - TMR-based weight buffers - N-well guarded PD
	hard-errors	- in-pixel self-healing with localized annealing
functionality		- spike-based imaging - contrast enhancement - recognition, positioning, focus state analysis

Fig. 2. Proposed space imager architecture with key features summarized.

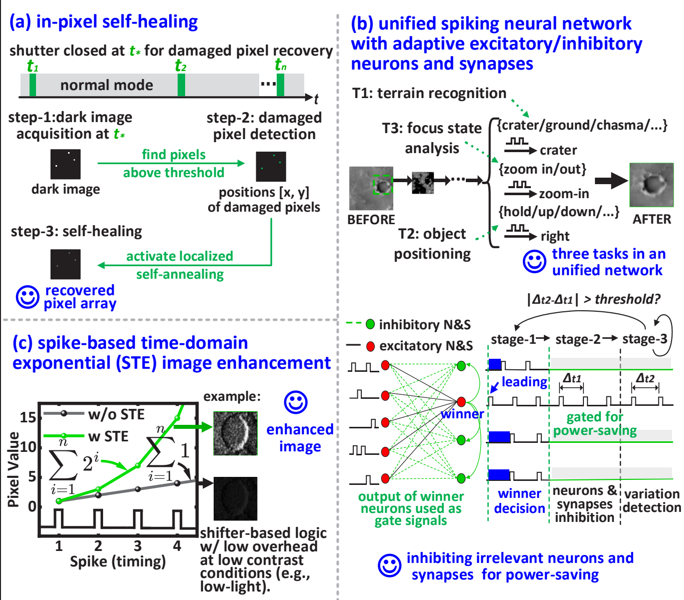

Fig. 3. Feature demonstration of the proposed space imager.

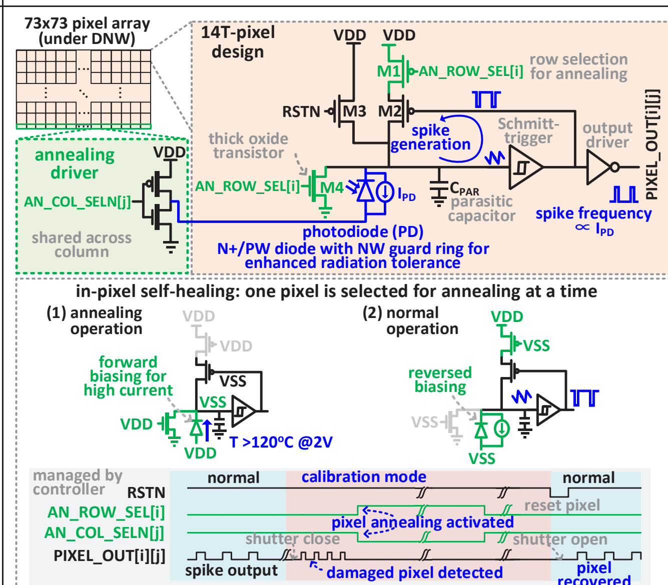

Fig. 4. Proposed spike-based pixel design (top) with localized self-annealing functionality (bottom).

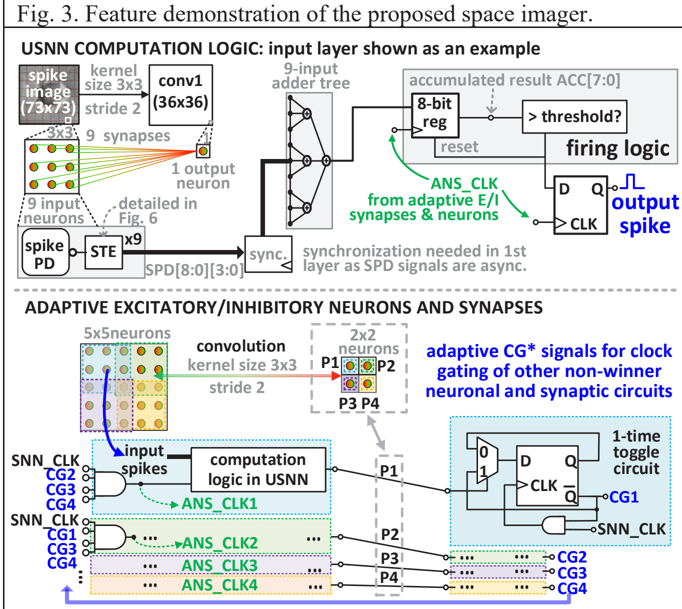

Fig. 5. Computation logic of unified spiking neural network (top) with adaptive excitatory/inhibitory neurons and synapses (bottom).

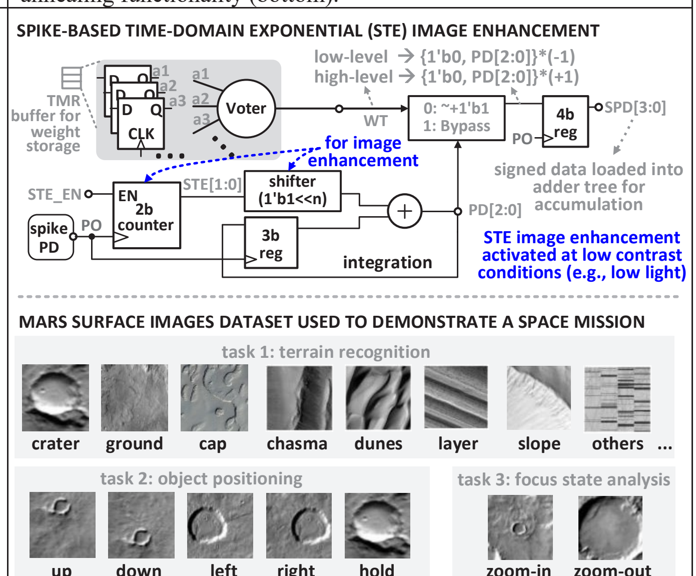

Fig. 6. Spike-based time-domain exponential (STE) image enhancement (top) and Mars surface images dataset (bottom).

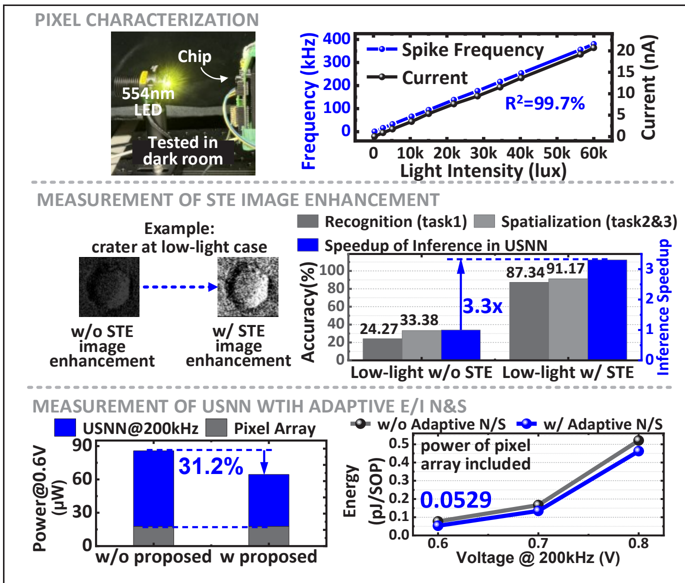

Fig. 7. Measurements: pixel characterization (top), STE enhancement (middle), USNN with adaptive E/I neurons and synapses (bottom).

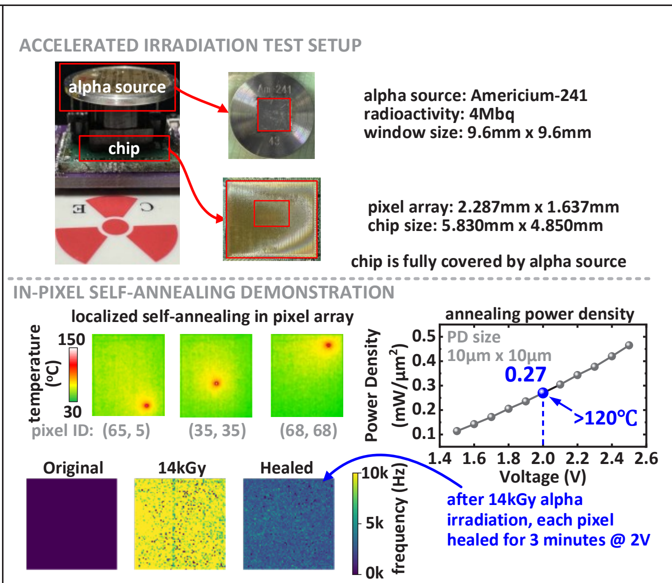

Fig. 8. Accelerated irradiation experiment setup (top), and in-pixel annealing demonstration (bottom).

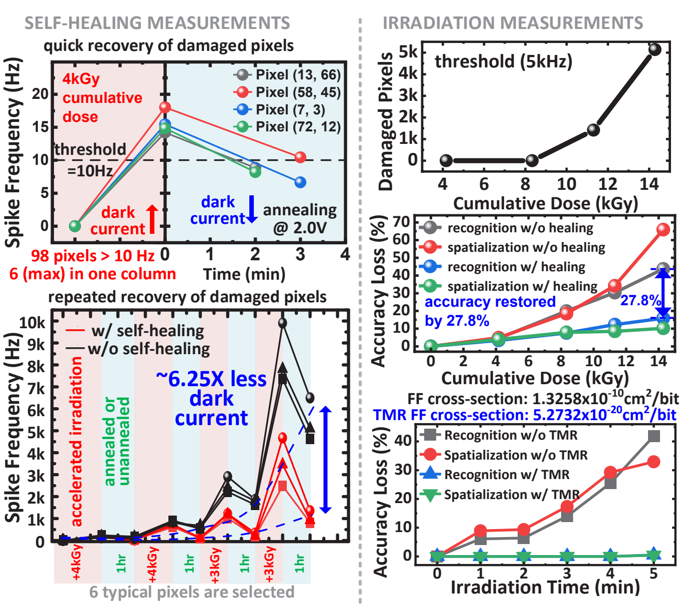

Fig. 9. Measurement results of accelerated irradiation experiments.

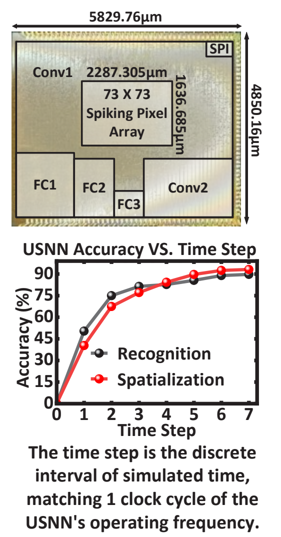

technology	180nm
chip architecture	Imager + SNN
chip size	5.83mm x 4.85mm (pixel array: 3.74mm²)
pixel array	73 x 73
pixel structure	14T spike
power	76.3µW @ 0.6V
image enhancement	spike-based time-domain exponential
radiation hardening of pixel	in-pixel self-healing via annealing (27mW/pixel @ 2.0V), NW-guarded PD
radiation tolerance capability	allowing for repeated recovery for pixels
neural network	unified SNN
precision	1-bit weight 4-bit activation
dataset (accuracy)	Mars surface images (89.77% for recognition; 93.18% for spatialization)
energy efficiency (TSOPS/W)	18.889 @ 0.6V
radiation hardening of NN	TMR FF cross-section: 5.2732x10⁻²⁰cm²/bit
energy	0.0529 pJ/SOP @ 0.6V

Fig. 10. Die micrograph and chip summary.

TABLE I. Comparison with state-of-the-art imagers

	[16] JSSC2023	[17] ISSCC2024	[11] commercial	[13] TNS2015	this work
technology	180nm CMOS	180nm CMOS	CIS	180nm CMOS	180nm CMOS
chip architecture	imager + CNN	imager + BNN	imager	imager	imager + SNN
supply voltage (V)	0.8	analog: 0.35 digital: 1.1	3.3 (normal), -9~-30 (V comp.)	analog: 3.3 digital: 1.8	0.6-0.8 (normal) **1.5-2.5 (self-healing)**
area (mm²)	5.368	25	> 75	not reported	28.275
pixel array	128x128	128x128	720x720	128x128	73x73
pixel size (um²)	7.6x7.6	20x20	12x12	10x10	22x21 (10x10 for PD)
pixel structure	4T PWM	6T PWM	not reported	3T	14T spike
power consumption	not reported	1.578~121.74mW	>0.2W	not reported	**76.3µW @ 0.6V**
image enhancement	No	No	No	No	**spike-based time-domain exponential**
pixel radiation hardening	-	-	high voltage compensation	gate-overlap PD, enclosed layout	**in-pixel self-healing,** NW-guarded PD
dark current increase @14kGy	-	-	not reported	>100x	**~125x w/o healing ~20x w/ healing**
neural network	CNN (3-layer)	optical + BNN (3-layer)	-	-	**USNN** (7-layer)
memory type	flip-flops	flip-flops			**TMR flip-flops**
frame/event rate	50~250 fps	1~32 fps	-	-	1~5,000 event/s @1~50k lux lighting
dataset (accuracy)	LFW / Kaggle Oregon Wildlife (93.6%)	MNIST (96.4%), Eyes Orientation (94.9%)	-	-	Mars Surface Images (89.77% recognition; 93.18% spatialization)
energy efficiency	-	0.367 TOPS/W	-	-	**18.889 TSOPS/W**
energy per operation	33.8 pJ/pixel/frame	-	-	-	**0.0529 pJ/SOP**

References

[1] A. A. Omar *et al.*, *DeSE*, 2021, pp. 438-442.
[2] P. Pant *et al.*, *SMART*, 2022, pp. 19-25.
[3] D. S. Katz *et al.*, *Computer*, vol. 36, no. 1, pp. 52-61, 2003.
[4] F. Neukart, *Space Policy*, 101676, 2025.
[5] R. Smith *et al.*, *Robotics*, 2020, 9(4): 94.
[6] N. Lee *et al.*, *JATIS*, 2016, 2(4): 041207-041207.
[7] W. Bluethmann *et al.*, *Autonomous robots*, 2003, 14: 179-197.
[8] I. Kostavelis *et al.*, *JFR*, 2014, 31(1): 107-140.
[9] C. Virmontois *et al.*, *IEEE TNS*, 2011.
[10] J. Bogaerts *et al.*, *IEEE TED*, vol. 50, no. 1, pp. 84-90, 2003.
[11] Imageone. (n.d.). Radiation tolerant video camera.
[12] V. Goiffon *et al.*, *IEEE TNS*, 64(1): 45-53, 2017.
[13] V. Goiffon *et al.*, *IEEE TNS*, 62(6): 2956-2964, 2015.
[14] M. Tsutsumi *et al.*, *IEEE EDL*, 44(1): 100-103, 2023.
[15] J. -M. Belloir *et al.*, *IEEE TNS*, 63(4): 2183-2192, 2016.
[16] T. -H. Hsu *et al.*, *IEEE JSSC*, 58(11): 3266-3274, 2023.
[17] X. Wang *et al.*, *IEEE ISSCC*, 2024, pp. 116-118.
[18] J. H. Park *et al.*, *IEEE TBCAS*, 14(6): 1230-1240, 2020.
[19] Y. Liu *et al.*, *ISSCC*, 2024, pp. 484-486.
[20] J. Tang *et al.*, *Advanced Materials*, 2019, 31(49): 1902761.
[21] A. Chaudhuri *et al.*, *IEEE ITC*, 2019, pp. 1-10.
[22] Q. Xu *et al.*, *DATE*, 2021, pp. 1586-1591.